Finite length diocotron modes

T. J. Hilsabeck[a] and T. M. O'Neil
Physics Department, University of California at San Diego, La Jolla, California 92093

(Received 2 August 2000; accepted 30 October 2000)

Diocotron modes are discussed for a finite length nonneutral plasma column under the assumption of bounce averaged $\mathbf{E}\times\mathbf{B}$ drift dynamics and small Debye length. In this regime, which is common to experiments, Debye shielding forces the mode potential to be constant along field lines within the plasma (i.e., $\partial\delta\phi/\partial z=0$). One can think of the plasma as a collection of magnetic-field aligned rods that undergo $\mathbf{E}\times\mathbf{B}$ drift across the field and adjust their length so as to maintain the condition $\partial\delta\phi/\partial z=0$ inside the plasma. Using the Green function (for a region bounded by a conducting cylinder) to relate the perturbed charge density and the perturbed potential, imposing the constraint $\partial\delta\phi/\partial z=0$, and discretizing yields a matrix eigenvalue problem. The mode eigenvector $\delta N_{l,\omega}(r_j)\equiv\int dz\ \delta n_{l,\omega}(r_j,z)$ is the lth azimuthal Fourier component of the z-integrated density perturbation, and the frequency ω is the eigenvalue. The solutions include the full continuum and discrete stable and unstable diocotron modes. Finite column length introduces a new set of discrete diocotron-like modes. Also, finite column length makes possible the exponential growth of $l=1$ diocotron modes, long observed in experiments. The paper focuses on these two problems. To approach quantitative agreement with experiment for the $l=1$ instabilities, the model is extended to include the dependence of a particle's bounce averaged rotation frequency on its axial energy. For certain distributions of axial energies, this dependence can substantially affect the instability. [DOI: 10.1063/1.1340856]

I. INTRODUCTION

This paper provides a description of diocotron and continuum modes for a finite length nonneutral plasma column.[1] The plasma is confined in a Malmberg–Penning trap with the configuration shown in Fig. 1. The wall is a conducting cylinder of radius R that is divided axially into three sections, with the central section grounded and the two end sections held at a positive potential V (to confine a plasma of positive charges). The central section has an axial length of $2Z$ and the end sections extend to infinity. The plasma resides in the region of the central grounded section, with axial confinement provided by electrostatic fields and radial confinement by a uniform axial magnetic field.

Because the plasma is nonneutral, there is a substantial radial electric field, and the plasma experiences an $\mathbf{E}\times\mathbf{B}$ drift rotation, $\omega_E=-(c/Br)(\partial\phi_0/\partial r)$. Here, $\phi_0(z,r)$ is the equilibrium plasma potential, $\mathbf{B}=-\hat{\mathbf{z}}B$ is the magnetic field, and (z,θ,r) is a cylindrical coordinate system with the z axis coincident with the axis of the trap. For a plasma of positive charges, it is convenient to choose the magnetic field in the $-\hat{\mathbf{z}}$ direction; this makes the rotation frequency (and the mode frequencies) positive. The frequencies are the same for a plasma of negative charges if the sign of the confinement fields is reversed (i.e., $\mathbf{B}\rightarrow-\mathbf{B}$ and $V\rightarrow-V$).

The modes of interest are characterized by frequencies that are comparable to the rotation frequency (i.e., $\omega\sim\omega_E$). The other important dynamical frequencies are the cyclotron frequency, Ω_c, and the characteristic axial bounce frequency for a particle, ω_b. In accord with experiment,[2,3] we assume that the frequencies are ordered as $\Omega_c\gg\omega_b\gg\omega_E\sim\omega$. The mode evolution can then be treated with bounce average $\mathbf{E}\times\mathbf{B}$ drift dynamics.

Also in accord with experiment, we assume that the Debye length is small compared to the plasma dimensions (i.e., $\lambda_D\ll r_p,l_p$). At first glance, the two inequalities $\omega_b\gg\omega_E$ and $\lambda_D\ll l_p$ look contradictory, but they both can be satisfied provided $\omega_p/\Omega_c\ll\lambda_D/l_p$, where ω_p is the plasma frequency. Here, we have used $\omega_b\sim\overline{v}/l_p$, $\omega_E\sim\omega_p^2/\Omega_c$, and $\lambda_D=\overline{v}/\omega_p$, where $\overline{v}$ is the thermal velocity. The frequency ordering and the smallness of the Debye length justify a reduced description of the plasma. In this Zero Debye Length Reduced Description, the plasma cannot tolerate (shields out) any electric field $(\partial\phi/\partial z)$ along the magnetic field. The plasma density, $n(z,\theta,r,t)$, is constant along z within the plasma and drops abruptly to zero at the plasma ends (on the scale $\lambda_D\rightarrow0$). Along each field line, the plasma is characterized by a well-defined length $2L(\theta,r,t)$. For convenience, we use $L(\theta,r,t)$ for the half-length.

The plasma can be thought of as a collection of magnetic-field aligned rods that move across the field through $\mathbf{E}\times\mathbf{B}$ drift motion and adjust their length so that $\partial\phi/\partial z$ vanishes everywhere inside the plasma. We will see that this constraint is satisfied if $\partial\phi/\partial z$ vanishes on the plasma surface [i.e., for $|z|=L(\theta,r,t)$].

With $L(\theta,r,t)$ determined in this way, the plasma state is specified by the two-dimensional z-integrated density distribution

$$N(\theta,r,t)=\int_{-\infty}^{+\infty}dz\ n(z,\theta,r,t)=2\,n(\theta,r,t)L(\theta,r,t), \quad (1)$$

[a]Electronic mail: thilsabeck@ucsd.edu

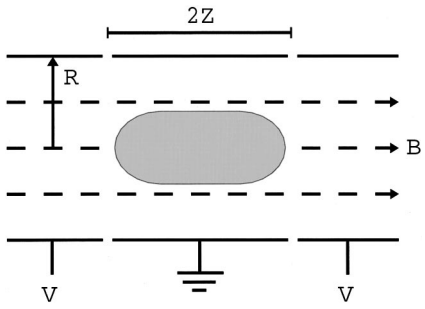

FIG. 1. Malmberg–Penning confinement geometry. The end cylinders extend out to infinity.

where $n(\theta,r,t)$ is the particle density inside the plasma. The electric potential $\phi(z,\theta,r,t)$ is expressed as a functional of $N(\theta,r,t)$ and $L(\theta,r,t)$ through an integral over a Green function for the trap geometry. The advantage of the reduced description is that it captures the three-dimensional nature of modes on a finite length plasma, while using a two-dimensional (2D) distribution to describe the plasma state.

To discuss the modes, this distribution is written as $N(\theta,r,t)=N_0(r)+\delta N_{l,\omega}(r)\exp(il\theta-i\omega t)$, where the first term describes the equilibrium and the second describes a mode. Likewise, $L(\theta,r,t)$ is written as the sum $L_0(r)+\delta L_{l,\omega}(r)\exp(il\theta-i\omega t)$, and the equations are linearized in $\delta N_{l,\omega}$ and $\delta L_{l,\omega}$. The analysis is implemented numerically, with functions evaluated at a set of discrete radial points $\{r_j\}$. The mode eigenvector $\{\delta N_{l,\omega}(r_j)\}$ is determined as the solution to a matrix eigenvalue problem, where the frequency ω is the eigenvalue. In the usual manner, eigenvectors for different eigenvalues are orthogonal, and a general linear solution can be written as a superposition of modes.

The set of modes includes what in an analytic theory would be called continuum modes as well as discrete modes. In this sense, the work extends recent work on 2D modes for an infinitely long column.[4]

We focus on two aspects of the modes that are due to finite column length. The first is the existence of a new set of discrete diocotron-like modes that appear in plasmas with very low shear in the rotational flow. The prototype of such a plasma is the uniform density plasma, for which the flow is a shear-free rigid rotation. It is well known that an infinitely long column of uniform density supports only one discrete diocotron-like mode for each azimuthal wave number.[1] In contrast, a uniform density column of finite length supports many additional discrete diocotron-like modes, with azimuthal phase velocities that are shifted from the rotation frequency by a small amount that depends on the plasma end shape. The shift tends to zero as the number of nodes in the radial eigenmode, $\delta N_{l,\omega}$, becomes large. A density variation in the equilibrium introduces shear in the rotational flow, and the new modes are absorbed into the continuum, as they become resonant with the fluid at some critical radius.

These new modes were predicted by Finn *et al.*,[5] who drew an analogy between the modes and Rossby waves in the quasigeostrophic β-plane approximation.[6] For analytic convenience, these authors approximated the plasma length by a quadratic function, $L_0(r)\simeq L_0(1-\kappa r^2)$, where κ is a measure of the end shape curvature at $r=0$. Neglecting any perturbation in the plasma length, they then obtained a simple dispersion relation for the modes that predicts a κ dependent shift in the azimuthal phase velocity (relative to the plasma rotation). The predicted frequencies are in qualitative agreement with our numerical results when the end shape is well-approximated by a quadratic function, but can differ significantly in other cases.

For example, the end shape can increase with radius on-axis (corresponding to negative curvature) and decrease with radius off-axis (corresponding to positive curvature). In this case, we find some modes that have a positive phase velocity shift and others that have a negative shift, whereas the dispersion relation predicts a single sign for the shift. The modes with negative shift ''live'' in a radial region where the equilibrium length is a decreasing function of radius, and the modes with positive shift live in the region where the length is increasing. The significance of the modes with positive shift is that they are more able to withstand small shear in the rotational flow. They rotate faster that the plasma.

Next we focus on a particular instability that exists because of finite column length. In general, a necessary condition for diocotron-like instabilities in an infinitely long column is that the column density, $n_0(r)$, be nonmonotonic in r.[1] For example, a hollow column satisfies this criterion. Likewise, a necessary condition for such instabilities in a finite length column is that $N_0(r)$ be nonmonotonic.[5,7] Detailed stability analyses for an infinitely long, hollow column have been carried out previously.[1,8] The modes for azimuthal mode number $l=1$ are special in that analytic solutions are possible for any density profile $n_0(r)$. Surprisingly, the analysis predicts that the $l=1$ modes are neutrally stable, that is, the imaginary part of the mode frequency ω is zero even for hollow columns.[9,10] An initial value solution of the infinite length, $l=1$ diocotron instability yields algebraic growth.[11] However, exponential growth of $l=1$ modes is observed experimentally for hollow columns of finite length.

Smith[12] predicted exponential growth when the plasma rotation frequency differs from that given by Gauss' law for an infinite column. He included a small shift in the rotation frequency arguing heuristically that it was due to the end confinement fields. Finn *et al.*[5] also considered this problem and obtained exponential growth. Again their analysis approximated the plasma length by a quadratic function. A mode induced perturbation in the plasma length was included for this analysis, but was implemented by a clever technique chosen for analytic convenience rather than experimental fidelity.

In contrast, our model accepts an arbitrary plasma shape and our axial boundary conditions are realistic. Also, our model incorporates the perturbation of the plasma length self-consistently using a Green function. Nevertheless, the two models find similar growth rates for plasmas with significant curvature.

Although consideration of finite length effects predicts the existence of an $l=1$ instability, good quantitative agreement with experiments has not been achieved. In general, the growth rates due to finite length effects alone are several times smaller than the experiments measure. Also, the calcu-

lated real frequencies are very near the maximum rotation frequency of the plasma, while the experiment may observe a frequency 25% lower.

In Sec. VII, we shall see that the incorporation of kinetic effects and the details of how the hollow columns are prepared have a significant impact on the instability. The important kinetic effect is the dependence of a particle's bounce averaged rotation frequency on its axial energy. The faster a particle strikes the end of the column, the larger radial electric force it experiences. Thus, a spread in axial particle energies produces a broadening of the unstable mode's resonance with the plasma rotation. In order to create the hollow profile columns, the axial confining potential is lowered and the highest energy particles escape. This process essentially cools the column near the trap axis and can significantly change the growth rate and frequency of the instability.

II. BASIC EQUATIONS

Because the cyclotron frequency is large and the cyclotron radius is small, the guiding center drift approximation can be used to follow the particle dynamics. Since the magnetic field is uniform, the guiding center drift Hamiltonian can be written as

$$H=\frac{p_z^2}{2m}+e\phi(z,\theta,p_\theta,t), \tag{2}$$

where the ordered pairs $(z,p_z=m\dot{z})$ and $(\theta,p_\theta=-eBr^2/2c)$ are canonically conjugate coordinates and momenta and ϕ is the electric potential.

Let $f=f(z,p_z,\theta,p_\theta,t)$ be the distribution of guiding centers. For convenience, we normalize f so that the total number of particles is given by

$$N=\frac{c}{eB}\int f dp_z dz d\theta dp_\theta=\int f dp_z d^3\mathbf{r}, \tag{3}$$

where $d^3\mathbf{r}=dzd\theta rdr$ is the configuration space volume element. The plasma density is then given by

$$n(z,\theta,r,t)=\int_{-\infty}^{+\infty} dp_z f. \tag{4}$$

Also for convenience, we will denote the radial dependence of various quantities interchangeably as $g(r)$ and $g(p_\theta)$, although different functional dependencies are implied for g in the two cases.

On the time scale of the modes, f evolves according to the collisionless drift kinetic equation

$$\frac{\partial f}{\partial t}+[f,H]=0, \tag{5}$$

where $[f,H]$ is a Poisson bracket

$$[f,H]\equiv\sum_i \frac{\partial f}{\partial q_i}\frac{\partial H}{\partial p_i}-\frac{\partial f}{\partial p_i}\frac{\partial H}{\partial q_i}.$$

The electric potential, ϕ, must be determined self-consistently from the Poisson equation and the boundary conditions specified for ϕ on the conducting wall of the trap. The solution can be written formally as

$$\phi(z,\theta,r,t)=\phi_T(z,r)+e\int_{-\infty}^{+\infty}dz'\int_0^{2\pi}d\theta'\int_0^R r'dr' \times G(z,\theta,r|z',\theta',r')n(z',\theta',r',t), \tag{6}$$

where $\phi_T(z,r)$ is the trap potential and $G(z,\theta,r|z',\theta',r')$ is a Green function that vanishes on the wall. Here, $\phi_T(z,r)$ satisfies the Laplace equation and matches the boundary conditions specified for ϕ on the wall. The second term (Green function term) satisfies the Poisson equation and vanishes on the wall, so the sum of the two provides the correct solution.

The Green function for the interior of an infinitely long, grounded, conducting cylinder, of radius R, is well-known[13]

$$G(z,\theta,r|z',\theta',r')=\frac{2}{R}\sum_{l=-\infty}^{+\infty}\sum_{n=1}^{\infty}\frac{e^{il(\theta-\theta')}J_l(\chi_{ln}r/R)J_l(\chi_{ln}r'/R)}{\chi_{ln}J_{l+1}^2(\chi_{ln})} \times e^{-(\chi_{ln}/R)(z_>-z_<)}, \tag{7}$$

or equivalently

$$G=\frac{2}{\pi}\sum_{l=-\infty}^{+\infty}\int_0^\infty dk e^{il(\theta-\theta')}\cos[k(z-z')]\frac{I_l(kr_<)}{I_l(kR)} \times[I_l(kr_>)K_l(kR)-K_l(kr_>)I_l(kR)], \tag{8}$$

where χ_{ln} is the nth zero of J_l. Here $z_>$ ($z_<$) is the greater (lesser) of z and z', and the same is true for the radial coordinate. In using the boundary condition for an infinitely long, grounded, conducting cylinder, we are assuming that the gaps in the electrodes are negligibly small. Furthermore, we assume the plasma column is always contained within the central conducting cylinder and that the length of the end cylinders is greater than their diameter. These conditions are experimentally typical. The sum over n in form (7) converges rapidly when $|z-z'|$ is large, and the k-integral in form (8) when $|r-r'|$ is large. For future reference, we note that G depends on (θ,θ') and (z,z') only through the combinations $\theta-\theta'$ and $z-z'$. This is a consequence of the rotational and translational invariance of the boundary conditions. In the following analysis, we will need the quantity

$$G_l(z,r|z',r')=\int_0^{2\pi}\frac{d(\theta-\theta')}{2\pi}e^{-il(\theta-\theta')}G. \tag{9}$$

Also, an expression for $\phi_T(z,r)$ is given by

$$\phi_T(z,r)=2V\sum_{n=1}^{\infty}\frac{J_0(\chi_{0n}r/R)}{\chi_{0n}J_1(\chi_{0n})}\cosh\left(\frac{\chi_{0n}z}{R}\right)e^{-(\chi_{0n}Z/R)}, \tag{10}$$

where V is the voltage on the end caps, R is the cylinder radius and Z is the central cylinder half-length. This expression is valid in the region $|z|<Z$.

III. EQUILIBRIA

We look for cylindrically symmetric equilibria setting $\phi=\phi_0(z,p_\theta)$ and correspondingly

$$H=H_0=\frac{p_z^2}{2m}+e\phi_0(z,p_\theta). \tag{11}$$

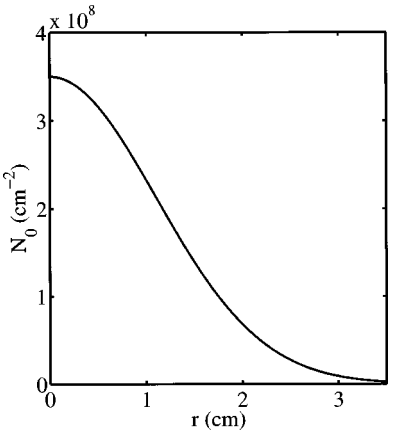

FIG. 2. Gaussian z-integrated density profile.

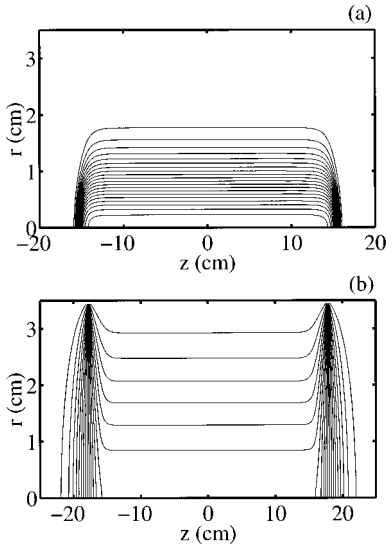

FIG. 3. Poisson–Boltzmann solution for constant density (a) and potential (b) contours ($R=3.5$ cm, $Z=17.3$ cm, $T=1$ eV).

Here, $\phi_0(z,p_\theta)$ is given by the sum of $\phi_T(z,r)$ and a cylindrically symmetrical space charge potential due to the Green function term in Eq. (6). Since $[p_\theta,H_0]$ vanishes, any distribution of the form $f=f_0(p_\theta,H_0)$ is an equilibrium.

To further specify the equilibrium, considerations beyond the collisionless drift kinetic equation must be taken into account. In the experiments of interest, modes are launched on both stable and unstable plasmas, and the preparation of the equilibrium is different in the two cases. For the stable case, the plasma is injected, held until collisions have established a local thermal equilibrium along each field line (a few collision times), and then modes are launched. The equilibrium for the stable modes is then the Boltzmann distribution

$$f_0(p_\theta,H_0)=\frac{N_0(p_\theta)\exp[-H_0/T(p_\theta)]}{\int_{-\infty}^{+\infty}dz\int_{-\infty}^{+\infty}dp_z\exp[-H_0(z,p_z,p_\theta)/T(p_\theta)]}, \tag{12}$$

where $T(p_\theta)$ is the local temperature along a field line at p_θ and $N_0(p_\theta)=\int_{-\infty}^{+\infty}dz\,n_0(z,p_\theta)$ is the z-integrated density along this field line. For given functions $N_0(p_\theta)$ and $T(p_\theta)$, Eq. (6) is an integral equation for the self-consistent potential, $\phi_0(z,r)$. A numerical solution for $\phi_0(z,r)$ can be obtained by iteration of Eq. (6), or of the Poisson equation itself. In turn, the solution for $\phi_0(z,r)$ completes the specification of the distribution $f_0(p_z,z,r)$ and the density $n_0(z,r)$.

In the limit where the Debye length is small, the solutions have a simple universal character. The charge density is arranged so that the component of the electric field along the magnetic field (i.e., $-\partial\phi_0/\partial z$) is Debye shielded out in the interior of the plasma. The potential is nearly constant along z and then rises abruptly at the plasma ends over a length scale of a few Debye lengths. As implied by Eq. (12), the density $n_0(z,r)$ is nearly constant along z and then falls off sharply near the ends.

As a specific example for numerical solution, we choose the z-integrated density $N_0(r)$ shown in Fig. 2, the radially independent temperature $T=1.0$ eV, the voltage on the end cylinders $V=60$ Volts (the central cylinder is grounded), and the trap aspect ratio $R/Z=5.086$. Figures 3(a) and 3(b) show contour plots for $\phi_0(z,r)$ and $n_0(z,r)$, and the behavior described in the previous paragraph is clearly visible. Away from the plasma ends the contours run parallel to the magnetic field (parallel to the z axis), but near the ends the contours cut across the field and are tightly bunched indicating a steep gradient. The gradient extends over a few Debye lengths.

For the case of unstable modes, the equilibrium is not of the Boltzmann form. In Sec. VII, we will discuss the preparation of the equilibrium for unstable modes in detail. Here, we need only the fact that the equilibrium distribution satisfies the inequality $\partial f_0/\partial H_0\leqslant 0$. This is the feature that is required for Debye shielding.

Incidentally, if $f_0(p_\theta,H_0)$ were not monotonically decreasing in H_0, the plasma would be subject to velocity space instabilities that would develop much more rapidly than the modes of interest here. Thus, basing a theory of low-frequency modes on the assumption $\partial f_0/\partial H_0\leqslant 0$ is not really a loss of generality.

To understand the connection of this assumption to shielding, first define the density

$$n_0[p_\theta,e\phi_0(z,p_\theta)]=\int_{-\infty}^{+\infty}dp_z f_0[p_\theta,p_z^2/2m+e\phi_0(z,p_\theta)], \tag{13}$$

and note that $\partial n_0/\partial e\phi_0=\int_{-\infty}^{+\infty}dp_z\partial f_0/\partial H_0$ is negative. The potential can be written as

$$\phi_0(z,r)=\phi_0(r)+\Delta\phi_0(z,r), \tag{14}$$

where the z-dependent part of $\Delta\phi_0(z,r)$ is presumed small in the plasma interior. This must be verified *a posteriori*. Taylor expanding the density with respect to $\Delta\phi_0$ and substituting into the Poisson equation yields the result

$$\left\{\frac{1}{r}\frac{\partial}{\partial r}r\frac{\partial\phi_0}{\partial r}+4\pi e n_0[r,\phi_0(r)]\right\}+\left\{\nabla^2\Delta\phi_0-\frac{1}{\lambda_D^2(r)}\Delta\phi_0\right\}=0, \tag{15}$$

where we have defined the effective Debye length

$$\frac{1}{\lambda_D^2(r)} \equiv \frac{4\pi e^2 n_0[r,\phi_0(r)]}{T(r)}, \tag{16}$$

in terms of the effective temperature

$$\frac{1}{T(r)} \equiv -\frac{1}{n_0}\frac{\partial n_0}{\partial e\phi_0}. \tag{17}$$

In writing $\lambda_D^2(r)$ as a positive quantity use has been made of the fact that $\partial n_0/\partial e\phi_0$ is negative.

We choose $\phi_0(r)$ so that the first bracket in Eq. (15) vanishes. The second bracket is then zero, so $\Delta\phi_0(z,r)$ satisfies the equation for Debye shielding. In the limit where the Debye shielding is small compared to the plasma dimensions, numerical solutions[14] show that $e\Delta\phi_0(z,r)/T$ is exponentially small in the plasma interior and grows exponentially as the plasma surface is approached, reaching the value $e\Delta\phi_0/T \sim 1$ at the surface. Near the surface an analytic solution is possible. $\Delta\phi_0(z,r)$ depends primarily on the coordinate ξ, measured along the local normal to the surface, so Eq. (15) reduces to the form

$$\frac{d^2}{d\xi^2}\Delta\phi_0 - \frac{1}{\lambda_D^2}\Delta\phi_0 = 0, \tag{18}$$

for which the solution is exponential growth on the spatial scale λ_D. When $e\Delta\phi_0/T$ reaches unity, the density drops (and the simple linearization procedure used here breaks down).

In the experiments of interest,[2,3] the Debye length is small compared to the plasma dimensions, so we develop a reduced description in which the Debye length is taken to the limit $\lambda_D \to 0$. The plasma then has a well-defined length along each field line $2L_0(r)$ and the density is given by

$$n_0(z,r) = \frac{N_0(r)}{2L_0(r)} U[L_0(r) - |z|], \tag{19}$$

where $U(x)$ is a step function. In this Zero Debye Length Reduced Description, the equilibrium is specified by the single function $N_0(r)$. The function $L_0(r)$ is determined by the requirement that $\partial\phi_0/\partial z = 0$ everywhere on the plasma surface, that is, for $|z| = L_0(r)$. The fact that $\partial\phi_0/\partial z$ vanishes on the surface implies that it vanishes throughout the plasma volume.

To prove this statement, note that the Poisson equation plus the z-independence of $n_0(z,r)$ inside the plasma implies the equation

$$\nabla^2 \frac{\partial\phi_0}{\partial z} = -4\pi e \frac{\partial n_0}{\partial z} = 0. \tag{20}$$

Since $\partial\phi_0/\partial z$ satisfies the Laplace equation throughout the plasma volume and vanishes on the plasma surface, it must vanish throughout the volume.

The method of obtaining $L_0(r)$ begins by recognizing that at each point along the correct equilibrium length function, the axial electric fields generated by the trap and the plasma exactly cancel. Should this condition not be satisfied, the plasma would expand or contract axially, until force balance is achieved. This heuristic dynamical description demonstrates the basic principle used to find the equilibrium length $L_0(r)$. Initially, $L_0(r)$ is approximated by some arbitrary, smooth curve $L_0^{(0)}(r)$ (usually a sphere). Next, the axial electric field is computed along this curve. The curve is then adjusted using the normalized electric force at the surface

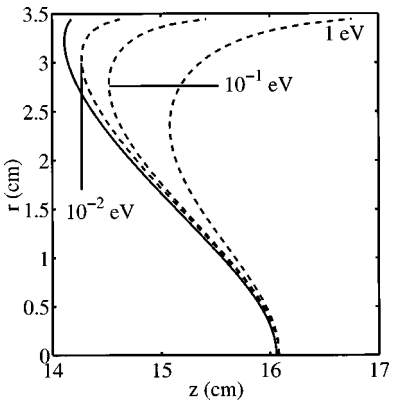

FIG. 4. Equilibrium plasma lengths for Poisson–Boltzmann solutions (dashed). Equilibrium plasma length for the Zero Debye Length Reduced Description (solid).

$$L_0^{(i+1)}(r) = L_0^{(i)}(r)\left[1 + \epsilon\frac{E_z^p[L_0^{(i)}(r),r] + E_z^t[L_0^{(i)}(r),r]}{E_z^p[L_0^{(i)}(r),r]}\right], \tag{21}$$

where E_z^t is the trap field, E_z^p is the plasma field, and ϵ is a small parameter chosen for convergence (usually one tenth). Here, the total electric field is normalized by the field due to the plasma in order to speed up convergence in region where the field is small (e.g., near the wall). This procedure is iterated until $L_0(r)$ is found [i.e., $L_0^{(n+1)}(r) = L_0^{(n)}(r)$].

The axial electric field component generated by the trap is obtained by differentiating the analytic expression for the potential in Eq. (10). The potential created by the plasma is given by the Green function from definition (7). The equilibrium plasma density is axisymmetric and uniform along the field lines. The potential produced by such a plasma inside a conducting cylinder is

$$\phi_p(z,r) = e\int_0^R 2\pi r'\,dr' \int_{-L_0(r')}^{L_0(r')} dz' \frac{N_0(r')}{2L_0(r')} \times G_0(z,r|z',r'), \tag{22}$$

where G_0 is defined in Eq. (9). The axial electric field is obtained by differentiating Eq. (22) with respect to z, and using the translational invariance of the Green function $(\partial/\partial z = -\partial/\partial z')$

$$-\frac{\partial\phi_p}{\partial z} = e\int_0^R 2\pi r'\,dr' \frac{N_0(r')}{2L_0(r')}\{G_0[z,r|L_0(r'),r'] - G_0[z,r|-L_0(r'),r']\}. \tag{23}$$

In Fig. 4, the zero temperature solution $|z| = L_0(r)$ obtained in this way is compared to a succession of Poisson–

Boltzmann solutions in which the temperature is varied. For each finite temperature solution, we define a half-density surface, $|z|=L_{1/2}(r)$, where

$$n[z=L_{1/2}(r),r]=\tfrac{1}{2}n(0,r). \tag{24}$$

The dashed curves in Fig. 4 are these surfaces for the sequence of temperatures ($T=1.0,0.1,0.01$ eV). The solid curve is the $T=0$ or Zero Debye Length Reduced Description solution. This comparison indicates that our equilibrium length function is a reasonable zero Debye length approximation to the plasma density for sufficiently low temperature. In the experiments of interest, the plasma temperature is typically 0.5 eV. In regions where the plasma density becomes small, the Debye length is large and our reduced description fails. However, we suppose that these low density regions have a small effect on the overall plasma dynamics.

IV. MODES

The unperturbed Hamiltonian $H_0=H_0(z,p_z,p_\theta)$ is integrable, so we can obtain a canonical transformation to action-angle variables. The first step is to define the bounce action as

$$I=\frac{1}{2\pi}\oint dz' p_z[z',H_0,p_\theta], \tag{25}$$

where $p_z[z,H_0,p_\theta]$ is obtained by solving Eq. (11) for p_z. Both H_0 and p_θ are held constant while carrying out the integral. A generating function for a canonical transformation from (z,p_z,θ,p_θ) to (ψ,I,Θ,P_Θ) is given by

$$W=\int_0^z dz' p_z[z',H_0(I,P_\Theta),P_\Theta]+\theta P_\Theta. \tag{26}$$

Taking partial derivatives in the prescribed manner[15] yields the transformation

$$\psi=\frac{\partial W}{\partial I}=\int_0^z \frac{dz'}{v_z[z',H_0,P_\Theta]}\frac{\partial H_0}{\partial I}, \tag{27}$$

$$p_\theta=\frac{\partial W}{\partial \theta}=P_\Theta, \tag{28}$$

$$\Theta=\frac{\partial W}{\partial P_\Theta}=\theta+\int_0^z \frac{dz'}{v_z[z',H_0,P_\Theta]} \times\left[\frac{\partial H_0(I,P_\Theta)}{\partial P_\Theta}-e\frac{\partial \phi_0(z,P_\Theta)}{\partial P_\Theta}\right]. \tag{29}$$

Here, use has been made of the relation $\partial p_z/\partial H_0=1/v_z$.

In Eq. (29), the bracket

$$\left[\frac{\partial H_0(I,P_\Theta)}{\partial P_\Theta}-e\frac{\partial \phi_0(z,P_\Theta)}{P_\Theta}\right]\equiv\delta\omega_E, \tag{30}$$

is the difference between the bounce averaged rotation frequency and the instantaneous rotation frequency. The second term on the right in Eq. (29) is no larger than $\delta\omega_E/\omega_b$, which is small according to our assumed ordering ($\omega_b \gg \omega_E$). Thus, we drop the second term and set $\Theta\simeq\theta$. For convenience, we continue to use the old variables p_θ and θ.

Since the transformation is canonical, the drift kinetic equation is still given by Eq. (5), but the Poisson bracket must be evaluated for the variables (ψ,I,θ,p_θ).

We assume that there is a small amplitude mode characterized by the potential $\delta\phi(z,\theta,p_\theta,t)$. The Hamiltonian is then given by

$$H=H_0(I,p_\theta)+\delta H(\psi,I,\theta,p_\theta,t), \tag{31}$$

where $\delta H=e\,\delta\phi$. The perturbation in the Hamiltonian gives rise to a perturbation in the distribution $\delta f(\psi,I,\theta,p_\theta,t)$. Linearizing the drift kinetic equation in the smallness of the perturbation yields

$$\frac{\partial \delta f}{\partial t}+[\delta f,H_0]+[f_0,\delta H]=0. \tag{32}$$

By taking into account the functional dependence $H_0=H_0(I,p_\theta)$ and $f_0=f_0(I,p_\theta)$, the equation can be rewritten as

$$\left[\frac{\partial}{\partial t}+\frac{\partial H_0}{\partial I}\frac{\partial}{\partial \psi}+\frac{\partial H_0}{\partial p_\theta}\frac{\partial}{\partial \theta}\right]\delta f-\frac{\partial \delta H}{\partial \psi}\frac{\partial f_0}{\partial I}-\frac{\partial \delta H}{\partial \theta}\frac{\partial f_0}{\partial p_\theta}=0. \tag{33}$$

Finally, by using $\partial f_0/\partial I=(\partial H_0/\partial I)(\partial f_0/\partial H_0)$ we obtain the result

$$\frac{\partial H_0}{\partial I}\frac{\partial}{\partial \psi}\left(\delta f-\delta H\frac{\partial f_0}{\partial H_0}\right)+\left(\frac{\partial}{\partial t}+\frac{\partial H_0}{\partial p_\theta}\frac{\partial}{\partial \theta}\right)\delta f-\frac{\partial \delta H}{\partial \theta}\frac{\partial f_0}{\partial p_\theta} =0. \tag{34}$$

We solve this equation through an expansion in the small parameter $\omega_E/\omega_b\sim\omega/\omega_b\ll 1$, where $\omega_b=\partial H_0/\partial I$ is the axial bounce frequency, $\omega_E=\partial H_0/\partial p_\theta$ is the rotation frequency and $\partial/\partial t\sim\omega$ is the characteristic frequency of the modes. In zero order, the equation reduces to the form

$$\frac{\partial H_0}{\partial I}\frac{\partial}{\partial \psi}\left(\delta f-\delta H\frac{\partial f_0}{\partial H_0}\right)=0, \tag{35}$$

which has the solution

$$\delta f-\delta H\frac{\partial f_0}{\partial H_0}=\left\langle \delta f-\delta H\frac{\partial f_0}{\partial H_0}\right\rangle_\psi, \tag{36}$$

or equivalently

$$\delta f=\langle \delta f\rangle_\psi+(\delta H-\langle \delta H\rangle_\psi)\frac{\partial f_0}{\partial H_0}. \tag{37}$$

Here, the bracket $\langle g\rangle_\psi(I,\theta,p_\theta,t)$ is the ψ-average $(\frac{1}{2}\pi)\int_0^{2\pi}d\psi\, g(\psi,I,\theta,p_\theta,t)$, where (I,θ,p_θ,t) are held constant in evaluating the integral. For each (I,θ,p_θ,t), solution (37) determines the ψ-dependence of $\delta f(\psi,I,\theta,p_\theta,t)$ relative to the ψ-average $\langle \delta f\rangle_\psi(I,\theta,p_\theta,t)$. To obtain an equation for $\langle \delta f\rangle_\psi$, we integrate Eq. (34) over ψ, projecting out the large first term. The result is

$$\left(\frac{\partial}{\partial t}+\frac{\partial H_0}{\partial p_\theta}\frac{\partial}{\partial \theta}\right)\langle \delta f\rangle_\psi=\frac{\partial\langle \delta H\rangle_\psi}{\partial \theta}\frac{\partial f_0}{\partial p_\theta}. \tag{38}$$

In the Zero Debye Length Reduced Description for the equilibrium, the transformation $(\psi,I,\theta,p_\theta)\rightarrow(z,p_z,\theta,p_\theta)$ is such that z-dependence for a function enters only through

ψ-dependence. Thus, Eq. (37) implies that all z-dependence in the perturbation δf is included in the term

$$e(\delta\phi-\langle\delta\phi\rangle_\psi)\frac{\partial f_0}{\partial H_0}=e\,\delta\phi'\frac{\partial f_0}{\partial H_0}, \tag{39}$$

where $\delta\phi'\equiv(\delta\phi-\langle\delta\phi\rangle_\psi)$ is the z-dependent part of the perturbed potential. In turn the z-dependent portion of the perturbed density, $\delta n=\int dp_z\delta f$, is given by

$$e\,\delta\phi'\frac{\partial n_0}{\partial e\phi_0}=-\frac{e\,\delta\phi'}{T(r)}n_0, \tag{40}$$

where $T(r)$ is the effective temperature defined in Eq. (17). Substituting this density perturbation into the Poisson equation shows that $\delta\phi'$ satisfies the equation for Debye shielding [see Eq. (18)]. Thus, we conclude that the mode perturbation exhibits such shielding (i.e., $\partial\delta\phi/\partial z\to 0$) in the plasma interior. Equation (37) then implies that δf and $\delta n=\int dp_z\delta f$ are independent of z (or ψ) in the plasma interior. Within a few Debye lengths of the end, $|\partial\delta\phi/\partial z|$ can become large, either adding to or subtracting from $\partial\phi_0/\partial z$ and, thereby, increasing or decreasing the plasma length locally.

These are the conclusions that are necessary to extend the Zero Debye Length Reduced Description to include modes. We allow for an increment to the plasma half-length, $L(\theta,r,t)=L_0(r)+\delta L(\theta,r,t)$, and for an increment to the z-integrated density, $N(\theta,r,t)=N_0(r)+\delta N(\theta,r,t)$. Substituting these expressions into Eq. (19) and linearizing yields the density increment

$$\delta n(z,\theta,r,t)=\left[\frac{\delta N(\theta,r,t)}{2L_0(r)}-\frac{N_0(r)}{2L_0(r)}\frac{\delta L(\theta,r,t)}{L_0(r)}\right]U[L_0(r)-|z|]+\frac{N_0(r)\,\delta L(\theta,r,t)}{2L_0(r)}\delta[L_0(r)-|z|], \tag{41}$$

where the delta function in the second term enters through the Taylor expansion for the step function. This term represents a surface shell of density increment associated with the length increment.

From Eq. (6), we obtain the relation

$$\delta\phi(z,\theta,r,t)=e\int_{-\infty}^{+\infty}dz'\int_0^{2\pi}d\theta'\int_0^R r'dr'\times G(z,\theta,r|z',\theta',r')\,\delta n(z',\theta',r',t). \tag{42}$$

Substituting for $\delta n(z',\theta',r',t)$ from Eq. (41) then provides an expression for $\delta\phi(z,\theta,r,t)$ as a linear functional of $\delta N(\theta,r,t)$ and $\delta L(\theta,r,t)$.

The length increment, $\delta L(\theta,r,t)$, is determined as a linear functional of $\delta N(\theta,r,t)$ by the requirement that $\partial\delta\phi/\partial z=0$ at $|z|=L_0(r)-$. Here, the minus sign indicates that the constraint $\partial\delta\phi/\partial z=0$ is to be imposed just inside the shell of surface charge [see second term in Eq. (41)]. Of course, the normal component of the electric field is discontinuous across a sheet of surface charge. One can show that this constraint implies that $\partial\delta\phi/\partial z$ vanishes throughout the plasma interior.

To include the effect of the modified length [i.e., $L_0(p_\theta)\to L_0(p_\theta)+\delta L(\theta,p_\theta,t)=L(\theta,p_\theta,t)$] in the Hamiltonian, we must use the modified length in the definition of the action, $I=(\frac{1}{2}\pi)\oint dz p_z=|p_z|2L(\theta,p_\theta,t)/\pi$. The Hamiltonian is then given by

$$H=\frac{I^2\pi^2}{8mL^2(\theta,p_\theta,t)}+e\phi(\theta,p_\theta,t), \tag{43}$$

where $\phi(\theta,p_\theta,t)$ is the z-independent potential inside the plasma. This Hamiltonian describes the bounce averaged transverse motion and assumes the ordering $\omega_b\gg\omega_E\sim\omega$. The ratio of the first term to the second is $T/e\phi_0\sim(\lambda_D/r_p)^2$, so in the limit of zero Debye length we drop the first term and set $H\simeq e\phi(\theta,p_\theta,t)$. We will discuss the effect of the first term in Sec. VII.

Just as the equilibrium is specified by the single function $N_0(r)$, the modes are specified by the single function $\delta N(\theta,r,t)$. The reduced description is completed by an equation for the evolution of $\delta N(\theta,r,t)$, which we obtain from Eq. (38). In this equation, we set $\omega_E=\partial H_0/\partial p_\theta=\partial e\phi_0/\partial p_\theta$ and $\langle\delta H\rangle=e\,\delta\phi(\theta,p_\theta,t)$, where $\phi_0(p_\theta)$ and $\delta\phi(\theta,p_\theta,t)$ are the z-independent equilibrium and mode potentials, respectively. Integrating Eq. (38) over $2\pi dI$ then yields

$$\left[\frac{\partial}{\partial t}+\omega_E(r)\frac{\partial}{\partial\theta}\right]\delta N(\theta,r,t)=-\frac{c}{Br}\frac{\partial\delta\phi}{\partial\theta}\frac{\partial N_0}{\partial r}(r), \tag{44}$$

where $\delta N=2\pi\int_0^\infty dI\langle\delta f\rangle_\psi$ and $N_0=2\pi\int_0^\infty dI f_0$.

To examine a single mode, we let perturbed quantities vary as $\exp(il\theta-i\omega t)$, so that Eqs. (41), (42), and (44) take the form

$$\delta n_{l,\omega}(z,r)=\left[\frac{\delta N_{l,\omega}(r)}{2L_0(r)}-\frac{N_0(r)}{2L_0(r)}\frac{\delta L_{l,\omega}(r)}{L_0(r)}\right]U[L_0(r)-|z|]+\frac{N_0(r)\,\delta L_{l,\omega}(r)}{2L_0(r)}\delta[L_0(r)-|z|], \tag{45}$$

$$\delta\phi_{l,\omega}(z,r)=e\int_{-\infty}^{+\infty}dz'\int_0^R r'dr'G_l(z,r|z',r')\times\delta n_{l,\omega}(z',r',t), \tag{46}$$

$$[\omega-l\omega_E(r)]\delta N_{l,\omega}(r)=\frac{cl}{Br}\frac{\partial N_0}{\partial r}\delta\phi_{l,\omega}(r), \tag{47}$$

where use has been made of definition (9). Finally, the length increment $\delta L_{l,\omega}(r)$ is determined as a functional of $\delta N_{l,\omega}(r)$ through the constraint

$$0=\left.\frac{\partial\delta\phi_{l,\omega}}{\partial z}\right|_{z=L_0(r)-}$$
$$=e\int_0^R r'dr'\left[\frac{\delta N_{l,\omega}(r')}{2L_0(r')}-\frac{N_0(r')\delta L_{l,\omega}(r')}{2L_0^2(r')}\right]$$
$$\times\{G_l[L_0(r)-,r|-L_0(r'),r']$$
$$-G_l[L_0(r)-,r|L_0(r'),r']\}$$
$$+e\int_0^R r'dr'\frac{N_0(r')\delta L_{l,\omega}(r')}{2L_0(r')}\left\{\frac{\partial G_l}{\partial z}[L_0(r)-,r|\right.$$
$$\left.-L_0(r'),r']+\frac{\partial G_l}{\partial z}[L_0(r)-,r|L_0(r'),r']\right\},\qquad(48)$$

where use has been made of the fact that G_l depends on z and z' only through the combination $z-z'$.

Before turning to the numerical implementation of these equations, we develop an orthogonality relation for the eigenmodes $\{\delta N_{l,\omega}(r)\}$ and discuss the representation of a general perturbation as a sum over the eigenmodes. We also obtain a necessary condition for instability [i.e., $\mathrm{Im}(\omega)=\gamma>0$]. These results are generalizations of similar results obtained earlier for the case of an infinitely long column.[1,4]

To start, we multiply Eq. (47) by $\delta n_{l,\omega'}(z,r)r/N_0'$ and integrate over $rdrdz$, to obtain the relation

$$\omega\int_0^R rdr\,\delta N_{l,\omega'}(r)\delta N_{l,\omega}(r)\left[\frac{1}{r}\frac{\partial N_0}{\partial r}\right]^{-1}$$
$$-l\int_0^R rdr\,\omega_E(r)\delta N_{l,\omega'}(r)\delta N_{l,\omega}(r)\left[\frac{1}{r}\frac{\partial N_0}{\partial r}\right]^{-1}$$
$$=\frac{cl}{B}\int_{-\infty}^{+\infty}dz\int_0^R rdr\,\delta\phi_{l,\omega}(r)\delta n_{l,\omega'}(z,r),\qquad(49)$$

where use has been made of the definition $\int_{-\infty}^{+\infty}dz\;\delta n_{l,\omega'}(z,r)=\delta N_{l,\omega'}(r)$ on the left-hand side. The function $\delta\phi_{l,\omega}(z,r)$ is equal to $\delta\phi_{l,\omega}(r)$ in the plasma interior, but can differ by order T in the end sheath. In our reduced description, where terms of order $T\to 0$ are neglected, $\delta\phi_{l,\omega}(r)$ can be replaced by $\delta\phi_{l,\omega}(z,r)$ in the integrand on the right-hand side of Eq. (49). By using the Green function relation (46), the right-hand side can be rewritten in a symmetric form

$$\omega\int_0^R rdr\,\delta N_{l,\omega'}(r)\delta N_{l,\omega}(r)\left[\frac{1}{r}\frac{\partial N_0}{\partial r}\right]^{-1}$$
$$-l\int_0^R rdr\,\omega_E(r)\delta N_{l,\omega'}(r)\delta N_{l,\omega}(r)\left[\frac{1}{r}\frac{\partial N_0}{\partial r}\right]^{-1}$$
$$=\frac{ec}{lB}\int_{-\infty}^{+\infty}dz\int_0^R rdr\int_{-\infty}^{+\infty}dz'\int_0^R r'dr'\,\delta G_l(z,r|z',r')$$
$$\times\delta n_{l,\omega}(z',r')\delta n_{l,\omega'}(z',r').\qquad(50)$$

A similar equation is obtained by interchanging ω and ω'. Subtracting the two equations yields the relation

$$0=(\omega-\omega')\int_0^R rdr\,\delta N_{l,\omega'}(r)\delta N_{l,\omega}(r)\left[\frac{1}{r}\frac{\partial N_0}{\partial r}\right]^{-1}.\qquad(51)$$

Thus, the eigenfunctions $\delta N_{l,\omega}(r)$ and $\delta N_{l,\omega'}(r)$ for which $\omega\neq\omega'$ satisfy the orthogonality condition

$$0=\int_0^R rdr\,\delta N_{l,\omega'}(r)\delta N_{l,\omega}(r)\left[\frac{1}{r}\frac{\partial N_0}{\partial r}\right]^{-1}.\qquad(52)$$

One might worry that the integrand diverges at a point where $[(1/r)(\partial N_0/\partial r)]$ passes through zero, but this is not the case. Equation (46) implies that $\delta N_{l,\omega}(r)$ and $\delta N_{l,\omega'}(r)$ are both proportional to $[(1/r)(\partial N_0/\partial r)]$, so in fact the integrand vanishes at a point where $[(1/r)(\partial N_0/\partial r)]$ passes through zero.

In the usual manner, a general perturbation can be expressed as a sum over the eigenmodes

$$\delta N(\theta,r,t)=\sum_{l,\omega}a_{l,\omega}\delta N_{l,\omega}(r)\exp[il\theta-i\omega t],\qquad(53)$$

where the orthogonality conditions (in r and θ) allow us to determine the coefficients $a_{l,\omega}$ in terms of the initial conditions

$$a_{l,\omega}=\frac{\int_0^R rdr[(1/r)(\partial N_0/\partial r)]^{-1}\delta N_{l,\omega}(r)\int_0^{2\pi}(d\theta/2\pi)\,e^{-il\theta}\delta N(\theta,r,t=0)}{\int_0^R rdr[(1/r)(\partial N_0/\partial r)]^{-1}\delta N_{l,\omega}^2(r)}.\qquad(54)$$

In Eq. (53), the sum over ω typically contains a continuum portion.

One caveat concerns the completeness of the set $\{\delta N_{l,\omega}(r)\}$ in the special case where $[(1/r)(\partial N_0/\partial r)]$ vanishes over a finite interval. Over this interval all of the $\{\delta N_{l,\omega}\}$ vanish, so sum (53) can represent only initial perturbations that vanish on the interval. Physically, this is not a problem, since all perturbations that arise through $\mathbf{E}\times\mathbf{B}$ drift dynamics [i.e., through Eq. (46)] satisfy this condition.

An easily obtained variant of Eq. (51) is the relation

$$0=(\omega-\omega'^*)\int_0^R rdr\,\delta N_{l,\omega'}^*(r)\delta N_{l,\omega}(r)\left[\frac{1}{r}\frac{\partial N_0}{\partial r}\right]^{-1}.\qquad(55)$$

Setting $\omega=\omega'=\omega_r+i\gamma$ and using Eq. (46) yields the result

$$0=\int_0^R rdr\,\frac{|l\,\delta\phi_l(r)|^2\gamma}{[\omega_r-\omega_E(r)]^2+\gamma^2}\frac{1}{r}\frac{\partial N_0}{\partial r}.\qquad(56)$$

Thus, instability ($\gamma>0$) is possible only if $\partial N_0/\partial r$ changes sign over the interval $[0,R]$. For a confined column, $\partial N_0/\partial r$

must be negative at large r, so instability requires that there be a region where $\partial N_0/\partial r>0$. This modified Rayleigh criterion has been found before[5,7] and has an analogy in the infinite length theory,[1,8] in which the z-integrated density is replaced by local density.

We emphasize that the condition $\partial N_0/\partial r>0$ is necessary, but not sufficient, for an instability. For example, a plasma with a length function that increases with radius near $r=0$ can have uniform local density, $n_0(r)=n_0$, and still have $\partial N_0/\partial r>0$ near the axis. Such a plasma is a shear-free global thermal equilibrium,[1,16] which is known to be stable.

V. NUMERICAL IMPLEMENTATION

The equations are discretized at radial points $\{r_i: i=1\cdots N\}$. The plasma state is completely determined by the vector $\{\delta N_{l,\omega}(r_i)\}$. The vector $\{\delta L_{l,\omega}(r_i)\}$ is determined by the discretized form of Eq. (48)

$$\sum_i A_{ji}\delta L_{l,\omega}(r_i)=\sum_i B_{ji}\delta N_{l,\omega}(r_i), \tag{57}$$

which can be inverted to obtain

$$\delta L_{l,\omega}(r_k)=\sum_{i,j} A^{-1}_{kj}B_{ji}\delta N_{l,\omega}(r_i).$$

Substituting this into Eq. (46) then yields an expression for the potential inside the plasma

$$\delta\phi_{l,\omega}(r_j)=\sum_i C_{ji}\delta N_{l,\omega}(r_i). \tag{58}$$

We can now form an eigenvalue equation using Eq. (47)

$$\omega\delta N_{l,\omega}(r_j)=l\omega_E(r_j)\delta N_{l,\omega}(r_j)+\frac{cl}{Br_j}\frac{\partial N_0}{\partial r_j}\sum_i C_{ji}\delta N_{l,\omega}(r_i). \tag{59}$$

This matrix can be diagonalized using standard techniques.

The difficulties encountered in the numerical implementation primarily concern the convergence of the Green function [see Eqs. (7) and (8)] and its axial derivative. The convergence of these expressions is provided by the spatial separation of the source and observation points. In form (7), the exponential ensures convergence when its argument becomes large compared with unity. For $n\gg 1$, $\chi_{ln}\sim n\pi$ and the number of terms required in the matrix element summation is roughly $R/|z-z'|$. This result illustrates the two main reasons for incurring additional computational costs. First, as the number of radial points is increased, the space between nearest neighbors is reduced and more terms will contribute in the summation. Therefore, increasing the spatial resolution to obtain greater accuracy will not only result in larger matrices, but the summation required to compute neighboring matrix elements converges more slowly as well. Second, as the size of the plasma is reduced with respect to the cylindrical wall, the spacing of grid points will also decrease. This implies that for a given number of discretization points, the eigenmode solution of smaller plasma requires more computation time. An example will illustrate this point. In Sec. VI A below, we compare our results to an analytic solution obtained by Dubin. Dubin's theory assumes a quadratic trap potential and neglects the image charges induced in the conducting wall. To satisfy these requirements in our system, we choose a small plasma whose radius is one tenth of the wall radius. The solution for such a plasma requires three times more cpu runtime than a similar plasma whose radius is one half of the wall radius, while 200 radial grid points are used in each case. The solution of the latter requires four minutes on a 300 MHz Pentium II.

We are not always guaranteed that summation in form (7) will converge for arbitrarily many terms. For example, nonmonotonic length functions may have $L_0(r_1)=L_0(r_2)$ for $r_1\neq r_2$. In this situation, the argument of the exponential vanishes and it becomes advantages to use the integral expression for the Green function in form (8). This integral converges due to the asymptotic behavior of the modified Bessel functions. For values of $k\gg 1$, the integrand varies as $k^{-1}\exp[-k(r_>-r_<)]$, which becomes small when $k>|r-r'|$. Therefore, the integral form of the Green function can be used to calculate matrix elements for which the summation in (7) fails or converges too slowly.

The discretized surface charge perturbation $\{\delta L(r_i)\}$ represents a series of ring charges located at $[r_i, L_0(r_i)]$. These coordinates are also the positions at which $\partial\delta\phi/\partial z$ is evaluated in constraint (48). When the charged ring source and the observation point are collocated, which is the case for the diagonal elements of A_{ji}, the electric field diverges. To avoid this situation, we note that in this instance the contribution from the image charge induced in the conducting wall is negligible. Therefore, this region of the plasma is well-approximated by the surface charge in free space which is produced upon rotating the line segment connecting neighboring grid points about the z axis. The field evaluation point is on the interior side of this surface and can be taken arbitrarily close. The axial electric field is dominated by the local surface charge and we may assume this field is adequately described as $\delta E_z=\hat{z}\cdot 2\pi\sigma\hat{n}$, where $\hat{n}$ is the inward normal to the surface.

In general, the accuracy of a numerical solution to a discretized equation is determined by the total number of evaluation points. Higher accuracy can be obtained at the cost of larger memory requirements and longer cpu runtimes. For this calculation, finer grids also increase the difficulty of performing the summations. As the grid spacing is decreased, more and more terms in the sums are needed for accurate evaluation of the matrix elements. In the solutions presented below no more than one million terms were kept in the summations. This was sufficient to compute matrices of order 400, and achieve convergence in the solutions. As is customary in the numerical solution of equations, convergence is assumed when a large increase in spatial resolution produces little or no change in the results.

VI. RESULTS

A. Comparison to Dubin modes

Although our model is analytically intractable for the general case, there is a special case for which we can compare our numerical results to the predictions of an analytic

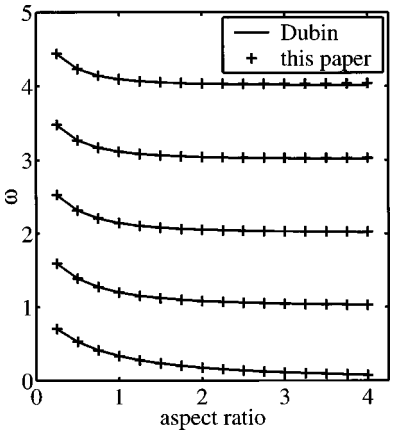

FIG. 5. Comparison to Dubin's analytic theory of small ($r_p = R/10$) spheroids. Mode frequencies are given for the first five azimuthal wave numbers and are normalized to the rotation frequency.

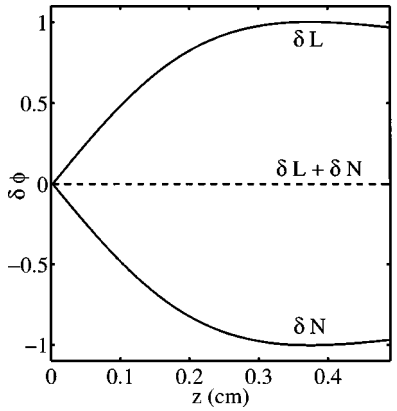

FIG. 6. Mode potentials along axis ($r = r_p/6$) produced by δN and δL (note: their sum cancels as expected).

theory. A small uniform density plasma that is confined in the central region of a trap, where the trap potential is nearly quadratic, has the shape of a spheroid. Using spheroidal coordinates and cold fluid theory, Dubin[17] obtained the complete spectrum of electrostatic modes. For a special class of these modes, the mode potential does not vary axially inside the plasma (i.e., $\partial \delta\phi/\partial z = 0$), so our numerical solutions should include these modes. Figure 5 compares our numerical solutions for the frequencies of these modes to the predictions of Dubin. The frequencies are plotted as a function of plasma aspect ratio (l_p/r_p), and results for the first five azimuthal mode numbers ($l = 1, \ldots, 5$) are shown. The results of our calculations are in excellent agreement with Dubin's predictions.

An important distinction between Dubin's analysis and ours is that he uses cold fluid theory and we use bounce averaged dynamics. Both of these approximations are useful, but they apply to different classes of experiments. Cold fluid theory requires the axial bounce frequency to be small (i.e., $\omega, \omega_E \gg \omega_b \to 0$), and bounce averaged dynamics requires it to be large (i.e., $\omega_b \gg \omega, \omega_E$). Note that both Dubin's analysis and ours assume that the Debye length is small. As mentioned earlier, it may seem that large bounce frequency and small Debye length are not compatible, but the two inequalities $\omega_b \gg \omega, \omega_E$ and $\lambda_D \ll l_p$ can both be satisfied provided that $\omega_p/\Omega_c \ll \lambda_D/l_p$. In cold fluid theory, the potential for a typical mode admits z-variation inside the plasma, whereas, such variation is prohibited (Debye shielded out) in our analysis. The fact that Dubin's analysis leads to a class of modes with no z-variation is presumably an accident of the spheroidal geometry.

A further check on the validity of our solutions concerns the Debye shielding condition. In our development, we assumed that the mode potentials are independent of axial position inside the plasma. This constraint is imposed by setting the z-electric field equal to zero just inside the surface. After solving for the modes, we can check to see that this was sufficient to guarantee z-independence throughout the plasma interior. Figure 6 plots the mode potentials due to the z-integrated density perturbation, the length perturbation, and their sum vs axial position along an arbitrary field line ($r = r_p/6$). The z-electric fields from the two perturbations cancel everywhere inside as expected. This consistency check has been verified for other modes and along other field lines as well.

B. New modes

One effect of finite column length is to introduce a new class of discrete diocotron-like modes for the case of plasmas with low shear in the rotational flow. The modes take their simplest form for a uniform density plasma, which is shear-free. An infinitely long column of uniform density supports only a single discrete diocotron-like mode for each azimuthal mode number.[10] In contrast, a finite length column of uniform density supports many additional discrete diocotron-like modes.

These modes were predicted by Finn *et al.*,[5] who drew an analogy between the new modes and Rossby waves in the quasigeostrophic β-plane approximation.[6] To obtain a simple equation for the modes, these authors set the perturbation in plasma length equal to zero (i.e., $\delta L_{l,\omega} = 0$). Although this approximation is not rigorously correct and we cannot expect quantitative agreement with the numerical results, the analysis captures the essence of the new modes and has the great advantage of simplicity.

Setting $\delta L_{l,\omega} = 0$ and using Eqs. (45) and (47) yields

$$4\pi e\, \delta n_{l,\omega}(r) = \frac{4l\omega_E}{l\omega_E - \omega}\, \kappa(r)\, \delta\phi_{l,\omega}(r), \tag{60}$$

where

$$\kappa(r) \equiv -\frac{1}{2rL_0(r)}\, \frac{\partial L_0}{\partial r}. \tag{61}$$

Inside the plasma, $\delta\phi_{l,\omega}(r)$ then satisfies the 2D Poisson equation

$$\frac{1}{r}\frac{d}{dr} r \frac{d\,\delta\phi_{l,\omega}}{dr} - \frac{l^2}{r^2}\, \delta\phi_{l,\omega}(r) + \frac{4l\omega_E}{l\omega_E - \omega}\, \kappa(r)\, \delta\phi_{l,\omega}(r) = 0. \tag{62}$$

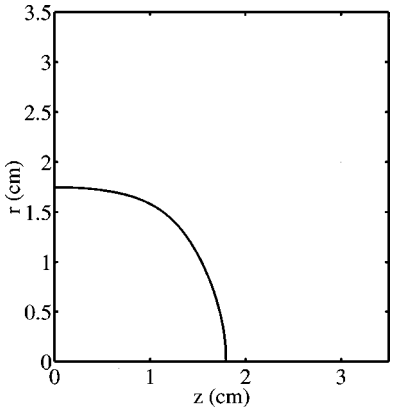

FIG. 7. Equilibrium length function for a uniform density plasma ($n_0 = 10^7$ cm^{-3}, $Z = R = 3.5$ cm, $V = 27$ Volts).

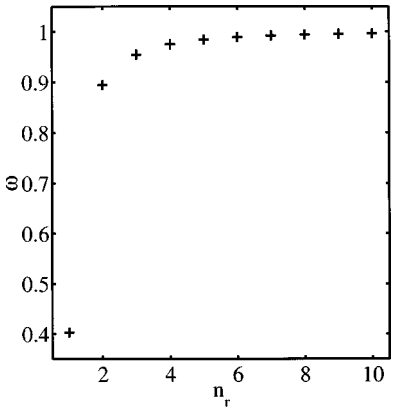

FIG. 8. $l = 1$ eigenmode frequencies for plasma shown in Fig. 7 (indexed by a radial wave number n_r).

As a further simplification, Finn *et al.* assume that $\kappa(r)$ is constant out to the wall at $r = R$. The solution is then given by a Bessel function.

$$\delta\phi_{l,\omega}(r) = AJ_l\left[\sqrt{\frac{4l\omega_E\kappa}{l\omega_E - \omega}}r\right], \tag{63}$$

and the boundary condition $\delta\phi_{l,\omega}(R) = 0$ then yields the dispersion relation

$$\omega - l\omega_E = -\frac{4l\omega_E\kappa R^2}{\chi_{ln}^2}, \tag{64}$$

where χ_{ln} is the nth zero of J_l. For κ positive corresponding to negative $L_0'(r)$, the modes are down shifted in azimuthal phase velocity from the plasma rotation frequency by a small amount that tends to zero as the number of radial nodes in the eigenfunction increases.

For a more realistic case where the plasma does not extend to the wall but κ is positive, Eq. (62) again describes a sequence of modes with phase velocities down shifted from the rotation frequency by a small amount tending to zero as the number of nodes increases. Of course, κ need not be positive everywhere. We will consider an example where κ is negative for small r and positive for large r. In this case, Eq. (62) implies two sets of new modes: A set with down shifted phase velocity that lives in the region of positive κ and a set with up shifted phase velocity that lives in the region of negative κ. The sign of the shift follows from the requirement that $\kappa/(l\omega_E - \omega)$ be positive for oscillatory solutions of Eq. (62). We find that these predictions are born out at least qualitatively by our numerical solutions of the full equations.

As a first example, we consider the $l = 1$ modes of a uniform density column in a trap characterized by $R = Z = 3.5$ cm and $V = 27$ Volts. Inside this trap we have a nonneutral plasma whose radius is 1.75 cm and whose uniform local density is $n_0 = 10^7$ cm^{-3}. The equilibrium length $L_0(r)$ is obtained using a slightly modified algorithm which maintains a constant local density as opposed to a constant z-integrated density and is shown in Fig. 7. Note that $L_0'(r)$ is negative corresponding to positive κ. As expected this plasma supports many new discrete eigenmodes in addition to the usual diocotron mode. Figure 8 shows the lowest ten eigenfrequencies (normalized to the plasma rotation frequency). The lowest frequency mode is the usual diocotron mode. Its eigenfunction is $\partial N_0/\partial r$ and its motion is a displacement of the column off-axis and the subsequent rotation of the entire column about the trap axis. Figure 9 gives the z-integrated density perturbations for the first three eigenmodes. The modes are indexed by a radial wave number n_r which indicates the number of radial nodes in the eigenfunction. As the radial index increases, the mode frequencies approach the rotation frequency. These modes are all discrete modes as opposed to continuum modes which exist for columns with shear in the rotational flow. Note that all the frequencies are lower than the rotation frequency of the column. This is a consequence of the monotonically decreasing length function (i.e., $\kappa > 0$).

There are equilibria whose length functions do not decrease monotonically with radius. Such equilibria can exist in standard Malmberg–Penning traps when the plasma radius is close to that of the trap. However, to better illustrate the effect of hollow end shape, we will consider a modified Malmberg–Penning trap in which two small ($r = R/50$) conducting rings are placed just outside the plasma ends and coaxial with the trap. To obtain significantly hollow end shapes, we bias the rings to an appropriate positive potential.

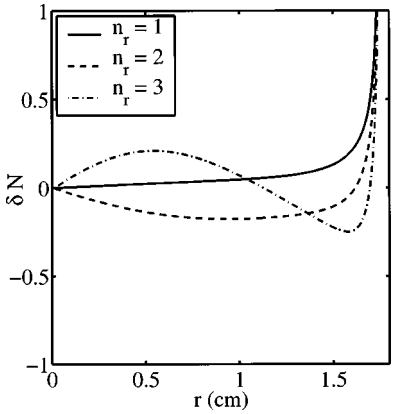

FIG. 9. Z-integrated density perturbations of the first three radial eigenmodes in Fig. 8.

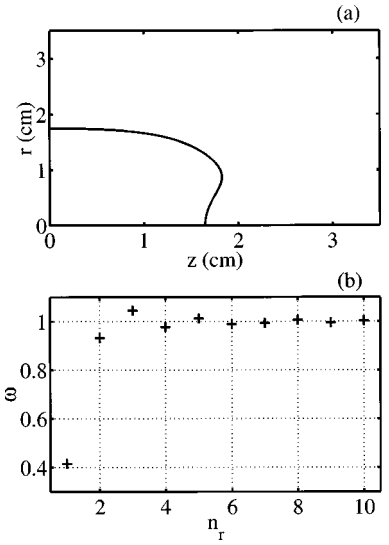

FIG. 10. (a) Hollow equilibrium length function ($R=Z=3.5$ cm, $V=27$ Volts). (b) Eigenfrequencies for hollow end shape column.

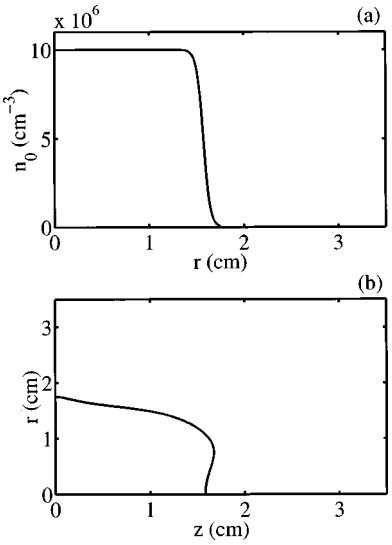

FIG. 11. Smoothed local density profile and hollow equilibrium length function ($R=Z=3.5$ cm, $V=21$ Volts).

In principle, we should also modify our Green function to account for the image charges induced on these rings by the mode perturbations. However, if the rings are sufficiently small we can safely ignore these images. Figure 10(a) shows a hollow end shape equilibrium. Here the uniform local plasma density is $n_0=10^7\,\mathrm{cm}^{-3}$, $R=Z=3.5$ cm, $V=21$ Volts and the additional conductors are located at $z=\pm 2.625$ cm. Figure 10(b) shows the eigenmode frequencies of the system. In addition to the slow modes discussed earlier, there are modes which rotate faster than the column. The presence of both slow and fast modes on the same column is a result of the length function having a radial derivative which changes sign. As expected, the density perturbations associated with the fast (slow) modes are localized where the length function is increasing (decreasing) with radius.

C. Shear profiles

The discrete modes of a rigid rotor plasma can be destroyed by the introduction of shear into the $\mathbf{E}\times\mathbf{B}$ flow. For an infinite length column, the $l>1$ diocotron modes are absorbed into the continuum[18] when they become resonant with the plasma rotation frequency.

Finite length columns also exhibit this phenomenon. As the local density profile is smoothed, the high n_r modes are absorbed into the continuum as they become resonant with the fluid. The z-integrated density eigenfunctions of these modes are no longer smooth functions indexed by a radial wave number, but become discontinuous at the resonant radius. For $l=1$, a plasma with significant shear and a monotonically decreasing length function retains only its center-of-mass discrete mode. All other eigenmodes are part of the continuum. Experimentally prepared profiles typically contain shear and this may explain why the higher order modes have not been observed.

For monotonically decreasing $n_0(r)$, only modes which rotate slower than the central rotation frequency will become resonant with the plasma rotation and are absorbed into the continuum. However, hollow end shape plasmas support modes with azimuthal phase velocities above the highest rotation frequency. These modes remain discrete in the presence of shear and may be observable experimentally. Figure 11(a) shows a local density profile which is constant throughout the column and falls smoothly to zero near the edge. Figure 11(b) is the equilibrium length function for this density profile and is a nonmonotonic function of radius. In Fig. 12(a), we plot the spectrum of eigenmodes for this system. Except for the lowest frequency center-of-mass mode, all of the discrete modes with frequencies lower than the central rotation frequency have become part of the continuum. The addition of more grid points will fill in the continuum with more modes. On the contrary, the modes which rotate faster than the plasma are discrete and remain separated from each other by fixed frequency intervals as the spatial resolution is increased. The z-integrated density per-

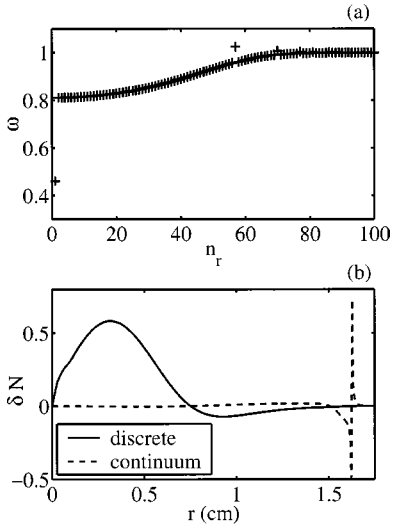

FIG. 12. (a) Spectrum of eigenmodes. (b) Eigenfunctions for the highest frequency mode and a continuum mode.

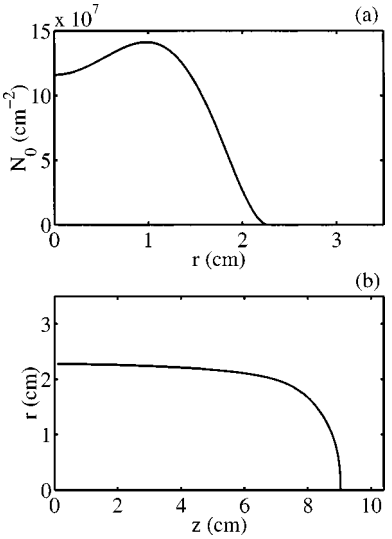

FIG. 13. Hollow z-integrated density profile and calculated equilibrium length function ($R=3.5$ cm, $Z=10.4$ cm, $V=60$ Volts).

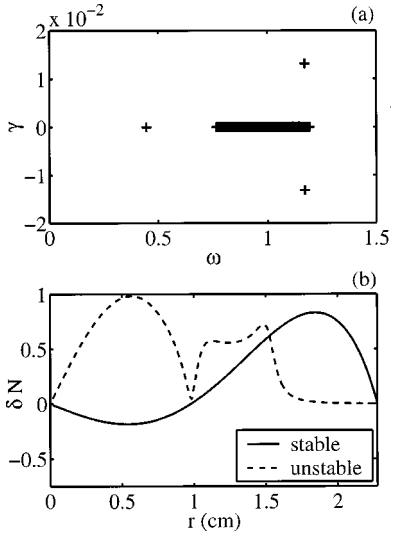

FIG. 14. Spectrum of eigenmodes and eigenfunctions for stable and unstable modes (note: unstable mode eigenfunction shown is $|\delta N|$).

turbations for the fastest mode and one of the discrete modes are shown in Fig. 12(b). The solid curve represents the fast, discrete eigenmode. The perturbation is most prominent for small radii where the length function is increasing with radius and is smallest at larger radii where the length function is decreasing. The dashed curve is a continuum eigenmode and exhibits the characteristic discontinuity at the resonant radius.

D. Diocotron instability for azimuthal mode number *l=1*

Another problem where finite column length plays an important role is the $l=1$ diocotron instability. As mentioned earlier, a necessary condition for diocotron instabilities is that $N_0(r)$ be nonmonotonic. For an infinitely long column, a normal mode analysis[9] predicts neutral stability [i.e., $\mathrm{Im}(\omega)=0$] for all $l=1$ modes, and an initial value analysis predicts the possibility of algebraic growth (i.e., $\delta n \propto \sqrt{t}$). However, experiments[2,3] clearly exhibit exponential growth for $l=1$ modes.

Smith[12] and Finn *et al.*[5] have argued theoretically that the exponential growth is due to finite column length. Likewise, our numerical solutions find the possibility of exponential growth for $l=1$ modes. However, we will find that quantitative agreement with the measured growth rates and frequencies requires the inclusion of a kinetic effect (see Sec. VII).

First we examine the results from the zero Debye length theory (no kinetic effect). Consider the z-integrated density profile in Fig. 13(a). Figure 13(b) shows the equilibrium length function calculated for $R=3.5$ cm, $Z=10.4$ cm, and $V=60$ Volts. The spectrum of eigenmode frequencies for this system is given in Fig. 14(a). We can clearly see the continuum, the discrete stable mode frequency and the two complex conjugate frequencies of the unstable mode. The eigenfunctions of the discrete stable mode and the unstable mode are shown in Fig. 14(b). The eigenfunction of the stable mode is $\partial N_0/\partial r$ and represents the usual center of mass mode. The unstable mode eigenfunction has a global character and vanishes at the radius where the z-integrated density is largest. The z-integrated density profile in Fig. 13(a) is a smooth fit to an experimental profile. The experiment measured a growth rate of 0.045 and a frequency of 0.99 [normalized to $\omega_E(0)=2\pi e n_0(0)c/B$]. These values are quite different than the computed values of 0.013 and 1.17. These discrepancies are common to other density profiles and length functions. We will return to this subject in Sec. VII.

Finn *et al.*[5] cite two finite length effects which contribute to the $l=1$ instability: Curvature in the end shape and variation in the plasma length due to the presence of the mode. Their growth rates due to curvature effects are compared with our results in Fig. 15 for two different hollow density profiles. The curvature κ [defined in Eq. (61)] is obtained by fitting the equilibrium length function to a quadratic near $r=0$. For large values of κ this is a reasonable approximation and the two theories obtain similar growth rates. As the end cap voltages are increased, the curvature near the trap axis

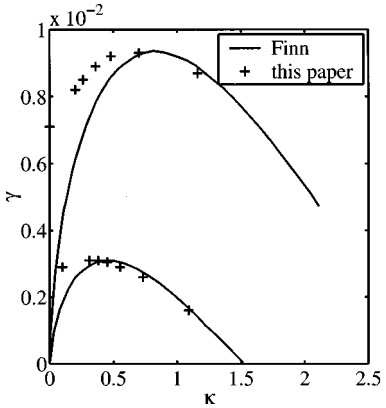

FIG. 15. Growth rate vs curvature comparison to the theory of Finn *et al.* (Ref. 5).

tends to zero and the results differ greatly. Finn *et al.*[5] also find that the perturbation of the plasma length is a source of instability and obtain finite growth rates for plasmas with zero curvature near $r=0$. However, the length perturbation is included by using a boundary condition that is chosen for analytical convenience rather that fidelity to the experimental geometry. Our method requires numerical implementation, but more accurately reflects the experimental geometry. This distinction makes comparison of growth rates due to length perturbations not possible.

Although the finite length theory calculations predict the existence of exponential instabilities in hollow columns, the quantitative agreement with the experiments is poor. The calculations consistently find growth rates 4 to 5 times smaller and real frequencies 20%–30% larger than the values measured in the experiments. However, these discrepancies may be the result of kinetic effects and the specific manner in which the hollow density profiles are created.

VII. KINETIC CORRECTIONS

In this section, we include a kinetic correction that can be important even though it is of order λ_D^2. Linearizing the Hamiltonian (43) with respect to $\delta\phi$ and δL yields $H=H_0+\delta H$, where

$$H_0=\frac{I^2\pi^2}{8mL_0^2(p_\theta)}+e\phi_0(p_\theta) \tag{65}$$

and

$$\delta H=e\,\delta\phi(\theta,p_\theta,t)-\frac{I^2\pi^2}{4mL_0^3(p_\theta)}\,\delta L(\theta,p_\theta,t). \tag{66}$$

Substituting into the kinetic equation (38) and decomposing into Fourier components in t and θ yields the result

$$\left[\omega_r+i\gamma-l\omega_E+\frac{lI^2\pi^2}{4mL_0^3(p_\theta)}\frac{\partial L_0}{\partial p_\theta}\right]\langle\delta f_{l,\omega}\rangle_\psi(p_\theta,I)$$
$$=-l\left[e\,\delta\phi_{l,\omega}(p_\theta)-\frac{I^2\pi^2}{4mL_0^3(p_\theta)}\,\delta L_{l,\omega}\right]\frac{\partial f_0}{\partial p_\theta}(p_\theta,I). \tag{67}$$

Since the mode of interest here is unstable, the mode frequency is expressed as a complex quantity explicitly ($\omega\rightarrow\omega_r+i\gamma$).

The term involving $\delta L_{l,\omega}$ is order $(\lambda_D/\Delta)^2$ smaller than the $\delta\phi_{l,\omega}$ term and can be ignored (Δ is the scale length on which the potential varies and is on the order of the plasma radius). However, the I-dependent term on the left-hand side must be kept since near the resonance $\omega_r-\omega_E$ vanishes and the growth rate γ is assumed to be small. Thus, we obtain

$$\langle\delta f_{l,\omega}\rangle_\psi=\frac{-le\,\delta\phi_{l,\omega}(\partial f_0/\partial p_\theta)}{\omega+i\gamma-l\omega_E+[lI^2\pi^2/4mL_0^3(p_\theta)](\partial L_0/\partial p_\theta)}. \tag{68}$$

Integrating over I and multiplying by $\omega_r+i\gamma-l\omega_E$ produces the kinetic eigenvalue equation

$$(\omega_r+i\gamma-l\omega_E)\,\delta N_{l,\omega}$$
$$=-le\,\delta\phi_{l,\omega}(\omega_r+i\gamma-l\omega_E)$$
$$\times\int_0^\infty\frac{2\pi dI\dfrac{\partial f_0}{\partial p_\theta}}{\omega_r+i\gamma-l\omega_E+\dfrac{lI^2\pi^2}{4mL_0^3(p_\theta)}\dfrac{\partial L_0}{\partial p_\theta}}. \tag{69}$$

Setting the term involving I in the denominator to zero results in the nonkinetic eigenvalue equation (47). The kinetic correction represents the dependence of the bounce averaged rotation frequency on the axial particle energy. In order to turn around at the ends, the fast particles must receive a larger impulse. Since the electric force providing this change in momentum is aligned normal to the surface of the plasma, there is both an impulse in z and in r provided the ends are not flat (note the dependence on the radial derivative of L_0). Therefore, particles with different axial energies have different bounce averaged rotation frequencies and plasma particles at several different radii can be in resonance with the unstable mode. We will show later that the new I-dependent term substantially affects the behavior of the unstable mode and is sensitive to the details of the particle distribution function.

The inclusion of the kinetic correction to the rotation frequency in our eigenvalue equation produces a matrix operator which depends functionally on the frequency of the eigenmode. Since the mode frequency is not known *a priori*, the discretized operator cannot be diagonalized directly. However, we are only considering one particular mode in the eigenspectrum and the kinetic correction to the eigenvalue of this mode is obtained using the following iterative technique. First, the nonkinetic unstable mode frequency, $\omega^{(0)}+i\gamma^{(0)}$ is substituted into the right hand side of Eq. (69). Next, the integral over I is performed. The result is a standard eigenvalue problem. After diagonalizing the resulting system of discretized equations, the adjusted unstable mode frequency, $\omega^{(1)}+i\gamma^{(1)}$, is identified. The new frequency is then substituted back into Eq. (69) and this procedure is repeated until the mode frequency converges to a stationary value. This method is successful provided the temperature is increased slowly. Also, this method will work for an arbitrary distribution function, since the integral over I may be performed numerically.

The distribution of axial particle velocities can be greatly affected by the experimental method used to create the hollow z-integrated density profiles. Initially, a monotonic column is created and held in the trap until local thermal equilibrium is established along the field lines. Therefore, the initial distribution of axial particle velocities is a Maxwellian and the temperature is typically uniform in radius. Using action-angle variables, the initial distribution takes the form

$$f_0^i(p_\theta,I)=\frac{N_0^i}{\sqrt{2\pi^3\overline{I}^2}}\exp\left(-\frac{I^2}{2\overline{I}^2}\right), \tag{70}$$

where $\overline{I}=(2L_0^i/\pi)(mT)^{1/2}$ and the superscript i stands for initial. The axial confining potential at one end is then low-

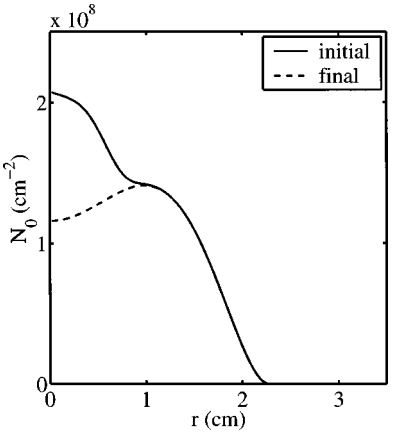

FIG. 16. An initial z-integrated density profile and the hollow profile obtained after ejection.

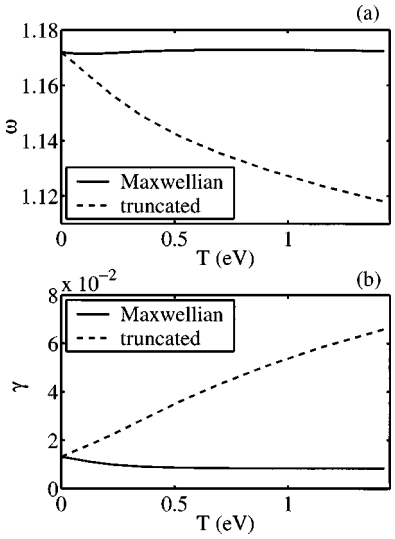

FIG. 17. Effects of finite temperature on the $l=1$ hollow profile instability [(a) real frequency, (b) growth rate] for a Maxwellian velocity distribution and the truncated distribution obtained from the profiles of Fig. 16.

ered and the more energetic particles escape from the trap. Since the plasma potential is highest (and the trap potential is lowest) on-axis, more particles are lost near the center and the resulting z-integrated density profile is hollow. In previous experiments, the confining potentials have been changed on a time scale comparable to a bounce period and the resulting distribution function of the hollowed column is not readily found.

In order to illustrate the effect the hollowing process can have on the instability, we will consider an experimental situation for which the distribution function is known. Specifically, the confining potential can be lowered and raised slowly with respect to a bounce period. Under such circumstances, the bounce action of the remaining particles is invariant. Therefore, the number of particles along a given field line with action $I \leqslant \hat{I}(p_\theta)$ remains fixed,

$$f_0^f(p_\theta, I) = \begin{pmatrix} f_0^i(p_\theta, I) & I \leqslant \hat{I} \\ 0 & I > \hat{I} \end{pmatrix}, \tag{71}$$

and the superscript f indicates final. The final distribution function is a truncated Maxwellian. In truth, the bounce action of particles near the separatrix is not conserved. Presumably, these nonadiabatic particles will smooth out the distribution function near the truncation point. However, results obtained for artificially smoothed distribution functions are not substantially different. Because the instability growth rate is larger than the collision frequency, the velocity distribution does not have a chance to relax back to a Maxwellian. The maximum action allowed on a field line, $\hat{I}(p_\theta)$, is determined from the initial and final z-integrated density profiles and the initial temperature.

$$\begin{aligned} N_0^f(p_\theta) &= \int_0^\infty 2\pi dI f_0^f(p_\theta, I) \\ &= \int_0^{\hat{I}(p_\theta)} 2\pi dI f_0^i(p_\theta, I) \\ &= N_0^i(p_\theta) \operatorname{erf}\left[\frac{\hat{I}(p_\theta)}{\sqrt{2I(p_\theta)}} \right]. \end{aligned} \tag{72}$$

The temperature and z-integrated density profiles can be measured experimentally and thus $\hat{I}(p_\theta)$ is known. Figure 16 shows two z-integrated density profiles. The solid curve represents a likely initial profile before the ejection process (the actual initial profile for this experiment was not measured). The dashed curve represents the final, hollow profile which supports the diocotron instability.

Figure 17 shows the corrections to the real frequency and the growth rate as the temperature increases. The solid lines represent the kinetic corrections for a plasma whose axial velocity distribution is a Maxwellian. In this case, the kinetic effects are insignificant. The dashed curves depict the corrections for a plasma with the truncated distribution defined by the profiles of Fig. 16. Here, the growth of the instability is greatly enhanced and the frequency is shifted down. In each case, the kinetic effects produced by the truncated distribution are substantially different than the nonkinetic results and the kinetic effects due to a Maxwellian distribution. This suggests that the instability cannot be completely understood in terms of density profiles alone.

Exact comparisons between the theory and experiments have not yet been made. The available experimental data on $l=1$ diocotron instabilities does not include the initial z-integrated density profiles before hollowing. Furthermore, the hollowing processes have not been adiabatic and the final distribution of axial energies is not known. However, corrections have been calculated for various probable initial profiles and different distribution functions. The results indicate the hollowing process can substantially affect the instability.

VIII. CONCLUSION

We have developed a Zero Debye Length Reduced Description for a nonneutral plasma column confined in a Malmberg–Penning trap. The critical assumption of this model is that the rapid bounce motion along field lines produces axial Debye shielding for the equilibrium and the low-

frequency diocotron modes. Using this model, an eigenvalue equation for linear diocotron modes was obtained for a finite length plasma column. A Green function formulation was used and the eigenmodes were obtained from a matrix diagonalization of the discretized system of equations.

The solutions revealed the existence of many discrete modes in rigid rotor plasmas not found in the infinite length theory. It was also shown that these are absorbed into the continuum when shear in the plasma rotation velocity produces resonances with the modes. Discrete modes rotating faster than the plasma were observed in hollow end shape plasmas. It was further demonstrated that these modes are not destroyed by a small amount of shear and might be observable experimentally.

We have also found instabilities for hollow density profile columns and verified that finite length columns are exponentially unstable even for $l=1$. Furthermore, we have shown that, in some cases, kinetic effects and the details of the axial velocity distribution function can have important consequences on the growth rate and real frequency of the unstable diocotron modes.

ACKNOWLEDGMENTS

The authors enjoyed useful discussions with A. Kabantsev, C. F. Driscoll, D. H. E. Dubin, D. A. Schecter, J. M. Finn, D. del-Castillo-Negrete, and G. Lapenta.

This work was supported by National Science Foundation Grant No. PHY-9876999 and Office of Naval Research Grant No. N00014-96-1-0239.

[1] R. C. Davidson, *Theory of Nonneutral Plasmas* (Benjamin, Reading, MA, 1974).
[2] C. F. Driscoll, Phys. Rev. Lett. **64**, 645 (1990).
[3] A. Kabantsev and C. Driscoll, in *Non-Neutral Plasmas III*, edited by J. Bollinger, R. Spencer, and R. Davidson (American Institute of Physics, New York, 1999), pp. 208–213.
[4] D. A. Schecter *et al.*, in *Non-Neutral Plasmas III*, edited by J. Bollinger, R. Spencer, and R. Davidson (American Institute of Physics, New York, 1999), pp. 115–122.
[5] J. M. Finn, D. del Castillo-Negrete, and D. C. Barnes, Phys. Plasmas **6**, 3744 (1999).
[6] R. Salmon, *Lectures on Geophysical Fluid Dynamics* (Oxford University Press, New York, 1998).
[7] T. M. O'Neil, Bull. Am. Phys. Soc. **40**, 1741 (1995).
[8] R. J. Briggs, J. D. Daugherty, and R. H. Levy, Phys. Fluids **13**, 421 (1970).
[9] R. H. Levy, Phys. Fluids **11**, 920 (1968).
[10] R. C. Davidson, *Physics of Nonneutral Plasmas* (Addison-Wesley, Redwood City, CA, 1990).
[11] R. A. Smith and M. N. Rosenbluth, Phys. Rev. Lett. **64**, 649 (1990).
[12] R. A. Smith, Phys. Fluids B **4**, 287 (1992).
[13] J. D. Jackson, *Classical Electrodynamics* (Wiley, New York, 1975).
[14] S. A. Prasad and T. M. O'Neil, Phys. Fluids **22**, 278 (1979).
[15] H. Goldstein, *Classical Mechanics* (Addison-Wesley, Reading, MA, 1980).
[16] D. H. E. Dubin and T. M. O'Neil, Rev. Mod. Phys. **71**, 87 (1999).
[17] D. H. E. Dubin, Phys. Rev. Lett. **66**, 2076 (1991).
[18] K. M. Case, Phys. Fluids **3**, 143 (1960).